Re-anchorage of a Ruptured Tendon in Bonded Post-Tensioned Concrete beams: Model validation

A. O. Abdelatif[1, a], J. S. Owen[1,b] and M. F. M. Hussein[1,c]

[1]Centre for Structural Engineering and Construction (CSEC)

Faculty of Engineering, University of Nottingham, University Park, Nottingham, NG7 2RD, UK

[a]evxaoa@nottingham.ac.uk, [b]john.owen@nottingham.ac.uk,
[c]mohammed.hussein@nottingham.ac.uk

Keywords: post-tensioned concrete; corrosion; rupture; re-anchorage; tendon; ESPI; assessment; residual structural capacity;

Abstract. Many post-tensioned concrete bridges have been reported to have ruptured tendons due to corrosion [1] and the assessment of their residual structural capacity has to account for the possibility of re-anchorage of failed tendons. This paper presents an experimental programme to validate a numerical model developed by the authors for the re-anchorage of a ruptured tendon in post-tensioned concrete [2]. The experimental programme considered 33 post-tensioned concrete prisms, in which the rupture of tendon was simulated by releasing the tendon at one end. The full field displacement at concrete surface after release was measured using 3D Electronic Speckle Pattern Interferometry (ESPI). A wide range of parameters: tendon diameter, duct material, grout strength, concrete strength and shear reinforcement were investigated to validate the proposed model, which is found to be suitable for use in assessing post-tensioned concrete bridges with damaged tendons.

Introduction

Corrosion of steel is one of the major threats to post-tensioned concrete structures. Numerous failures have been reported in post-tensioned concrete structures as a result of the rupture of their tendons due to corrosion, in some extreme cases leading to catastrophic failure [1, 3]. Therefore, serious attention should be given to the assessment of corroded post-tensioned structures. Once ruptured tendons have been identified, it is important to predict the residual capacity. As the ruptured tendon is able to re-anchor into the surrounding grout, it can contribute to the residual structural capacity of the structure [4, 5].

A number of structural assessment studies have used pre-tensioned models or empirical bond-slip relations to approximate the re-anchorage phenomenon [6, 7]. In some studies, re-anchoring of the ruptured tendon is completely neglected [8, 9]. This is attributed to the lack of models regarding the tendons' re-anchorage in post-tensioned concrete. The wrong estimation of the re-anchoring phenomenon of the ruptured tendon leads to an inaccurate prediction of the structural capacity of post-tensioned concrete structures after the rupture.

This paper presents part of a study aiming to predict the structural behaviour of post-tensioned concrete beams with ruptured tendons based on a novel model for the re-anchorage of a ruptured tendon developed by the authors [2]. The experimental validation of the model in [2] across different factors involved in the re-anchorage phenomenon is presented. The background to the re-anchorage of ruptured tendons is given first, and then a brief literature review on the experimental work is provided. This is followed by a description of the experiment, specimen properties, and measuring techniques. Finally the validation of the model is presented with conclusions on its application to the assessment of damaged structures.

Re-anchorage of the ruptured tendon

When the tendon is ruptured, its section at the point of rupture tries to return to its original diameter, so within the re-anchorage length, the tendon diameter varies as a result of Poisson's

effect forming a wedge shape [10]. The increase in diameter exerts a radial pressure onto the surrounding materials (i.e. grout, duct, and concrete). The exerted pressure produces a frictional component to the bond force which helps in transferring the force in the ruptured tendon gradually into the surrounding material over the re-anchorage length. This action is known as wedge action or the Hoyer effect [11]. It enhances the re-anchorage of the ruptured tendon and thus the structural capacity of the post-tensioned concrete element.

The authors developed an analytical model to describe the distribution of stress along the ruptured tendon [2] and a re-anchorage formula was proposed, Eq. (1).

$$x = \frac{r_s}{2\alpha\phi}\left[\left(\frac{1}{B}+\frac{\mu_s}{E_s}\frac{1}{B^2}\right)\ln\left(1+\frac{B}{A}f_s\right)-\left(\frac{1-\mu_s}{E_s}+\frac{\mu_s}{BE_s}\right)f_s\right] \quad (1)$$

Here f_s is the longitudinal stress in the tendon at a section, E_s is the Young's modulus of pre-stressing steel, r_s is the nominal radius of pre-stressing steel, ϕ is the coefficient of friction, μ_s is the Poisson's ratio of pre-stressing steel, α is the percentage of the prestressing steel surface area in contacted with the grout. A and B are constants that depend on the material and geometrical properties, they are calculated as shown in [2].

The model accounts for equilibrium and compatibility conditions at the steel-grout, grout-duct and duct-concrete interfaces as well as the effect of axial stresses in the post-tensioning steel and its confining materials, i.e. grout, duct and concrete. Formulation of the model is based on the elastic theory of thick-wall cylinders and the Coulomb friction law. The model was initially verified using an axi-symmetrical Finite Element (FE) model and compared with the UK Highway Agency's BA51/95 and previous experiments. One of the aims of this paper is to validate the proposed model experimentally using a wider range of parameters.

Experimental literature

Previously, a number of laboratory investigations have been carried out to study the bond behaviour between grout and the post-tensioning tendons as well as the performance of grouts of different qualities. However, limited experiments were conducted to understand the re-anchoring phenomenon of the ruptured tendon. In this section a brief literature review about the measuring techniques, rupture simulation, and the size of test specimen is presented.

Two measuring types of strain gauges were used in previous studies to monitor the strain changes, demountable mechanical (DEMEC) and electrical resistance. DEMEC strain gauges were used to investigate the effect of grout properties on transmission length on nineteen bonded post-tensioned concrete beams [12]. Electrical resistance strain gauges were used at the concrete surface to study tendon re-anchorage in curved beams [13] and during demolition [14, 15]. In some cases, the strain gauges were attached to the pre-stressing steel to monitor the tendons behaviour after rupture [7, 16]. However, there is a possibility in this approach that gauges may break due to tendon slippage after the rupture [7].

Because the corrosion process takes a long time, rupture due to corrosion has been simulated either by undoing nuts at the bar end [12] or by cutting the tendon through a prefabricated hole using a flame torch [13] or saw [7, 16]. Investigations were made on different size specimens, including real bridge girders [14, 15], laboratory beams with large cross section [13] and long spans (~10 m) [17], and on 3-5 meter beams with small cross section (i.e. < 500x500) [7, 12, 16].

The drawback of the previous experiments on the behaviour of the ruptured tendon can be summarized in three points:

- Conducting experiments on full scale or real bridge beams restricts the number of parameters to be varied for practical and cost issues.

- Taking point measurements of strain limits the number of the measuring points based on the specimen length.
- Simulating tendon rupture by saw cut might disturb the grout inducing cracks.

Experimental work

33 concrete prisms (500x100x100) with an embedded duct along the centre were prepared and then post-tensioned using a single smooth pre-stressing bar. A wide range of parameters was used in this study in order to validate the proposed model. These parameters include: initial pre-stress; tendon diameter; duct material; grout strength; concrete strength; shear reinforcement. The material properties, pre-stress, and support conditions for each prism are summarised in appendix A.

The pre-stressing load was controlled by means of a load cell and a bespoke extended anchor system at one end, Figure 1 and Figure 2, before the grout was injected. Tendon rupture was then simulated by releasing the nuts between the extended anchorage plates. Two different support setups were used to investigate the influence of the support position on the tendon's re-anchorage.

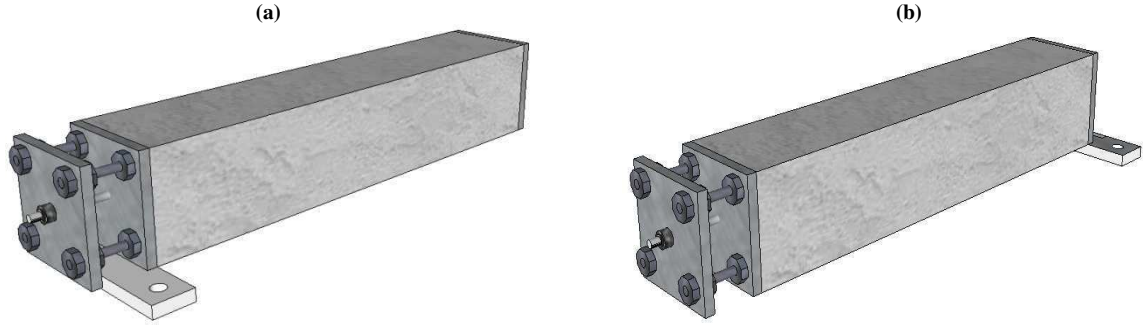

Figure 1: Specimen design: (a) Setup-1; (b) Setup-2

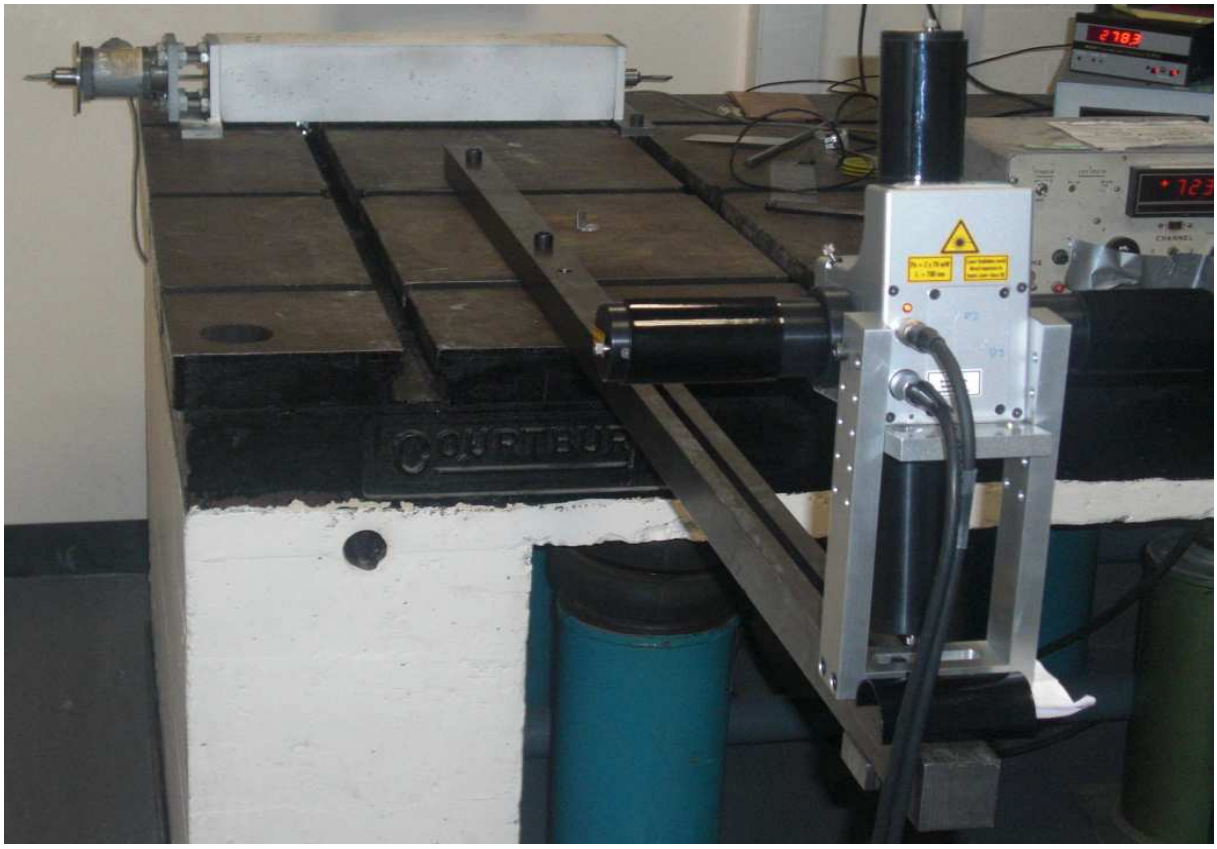

Figure 2: Test setup showing specimen and ESPI camera

Full field displacement measurements during the release of pre-stressed force were recorded using 3D Electronic Speckle Pattern Interferometry (ESPI), which is an optical, non-contact technique for measuring surface displacements. The prism surface was prepared by spraying with matt white paint and then illuminated by a laser to form a pattern known as laser speckle. Deformations of the surface as the tendon is released result in a change in the intensity distribution of the speckle pattern.

Figure 3 gives examples of the speckle pattern changing as the pre-stress is released in eight steps. These changes, which were recorded by the ESPI camera system shown in Figure 2, can then be used to extract surface displacements. The displacement of each point is calculated using image correlation techniques for the images throughout the releasing steps [18].

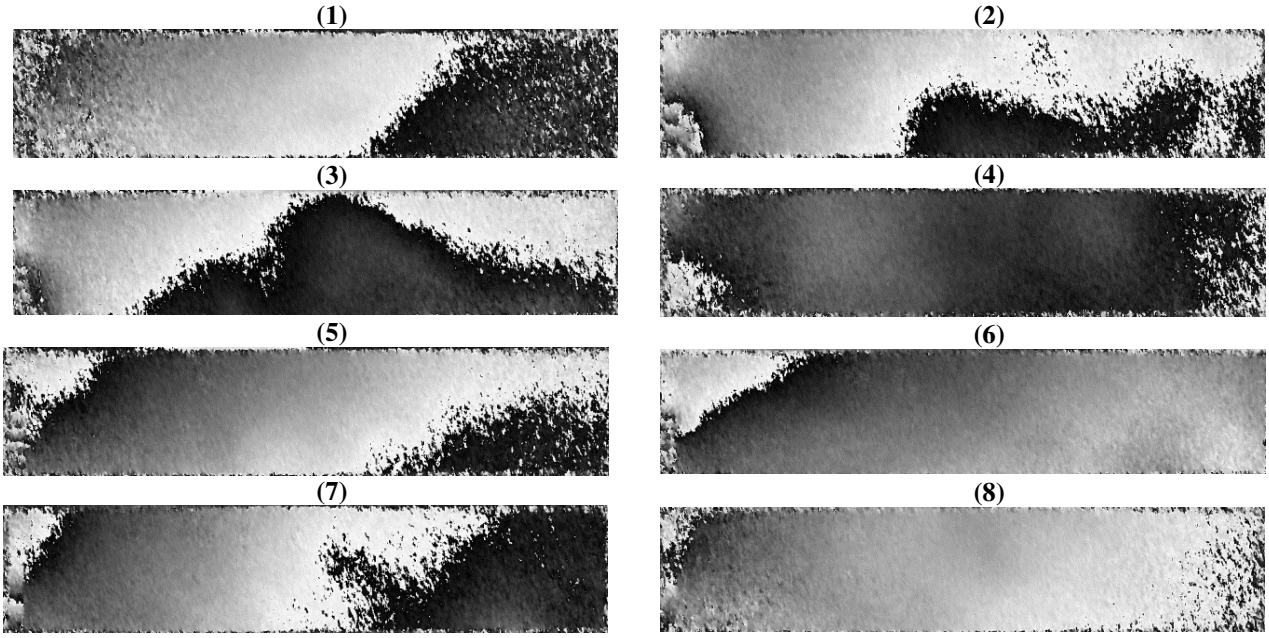

Figure 3: Variation of speckle pattern fringes through 8 load releasing steps (prism C2)

Results and discussions

As an example of typical results, the full field displacements in the longitudinal direction due to the release of pre-stress for prisms G2 and C20 are shown in Figure 4. These two prisms had different setups; prism G2 was fixed at the left lower corner while the C20 was fixed at the right lower corner. The post-tensioning force in both prisms was released at the extended anchor (i.e. at the left-hand end).

After the pre-stressing force has been released, the concrete expands due to the loss of compression force. The expansion takes place away from the fixed corner towards the far end.

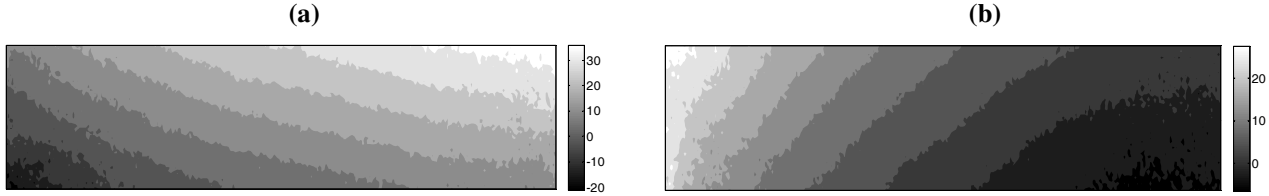

Figure 4: ESPI full field displacement (μm): (a) G2, fixed at left lower corner, (b) C20, fixed at right lower corner

From the full field displacement contours, the displacement profile at the level of the tendon can be extracted and plotted along the length of the prism as shown in Figure 5. The figure also demonstrates the consequence of the failure of the tendon on the concrete surface and how concrete expands after tendon rupture. Taking into account the proportion of stress to displacement, the

displacement profiles support the model hypothesis of non-linear stress distribution over the re-anchorage length [2].

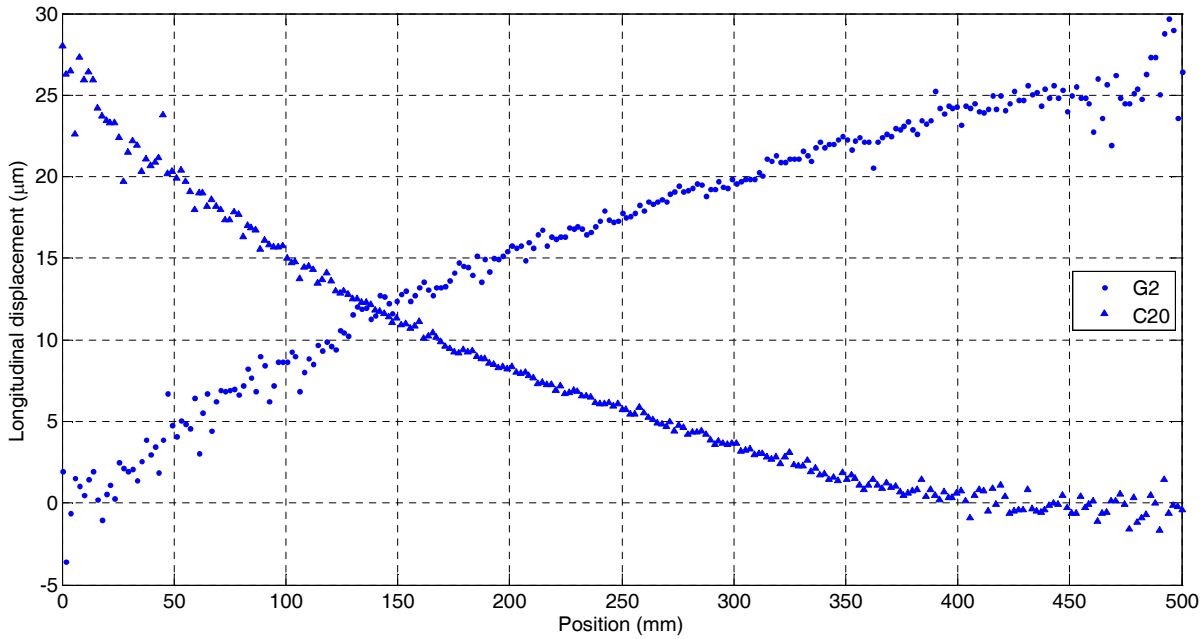

Figure 5: Displacement profile of prism G2 and C20 at the level of the tendon on concrete surface

Model validation. In order to validate the model against the experiments some assumptions have to be made to estimate the concrete surface displacement out of the model. Therefore it is assumed that the stress changes on pre-stressing tendon ($\Delta\sigma_s$) are proportioned to concrete stress (σ_c) and thereby to concrete displacement (δ_c).

$$\Delta\sigma_s \propto \sigma_c \tag{2}$$

and

$$\sigma_c \propto u_c \tag{3}$$

If the prism is supported at one end (*at* $x = x_i$), the displacement at each point ($u_c(x_n)$) will be:

$$u_c(x_n) = \sum_{x=x_n}^{x=x_i} \delta_c(x) \tag{4}$$

By making use of Eq. (3), the deformation of the concrete surface after tendon rupture predicted by the model can be compared against the ESPI experimental data (Figure 6). The deformations are calculated in the longitudinal direction at the level of the tendon and then normalised to the maximum deformation. Figure 6a, Figure 6b, and Figure 6c are sample results where the setup-1 is used and Figure 6d, Figure 6e, and Figure 6f for setup-2. In these results, the model predictions compare very well with the experimental data over a wide range of parameters.

Although the model does not account for the shear reinforcement, good agreement was found in a comparison between the model and post-tensioned concrete prisms with shear links (Figure 6d). This suggests that the impact of the shear reinforcement is negligible. This finding contradicts with previous observation during a controlled demolition of bonded post-tensioned concrete structures. More investigations would be made in future to scrutinise this finding.

ESPI limitations. One of the intrinsic limitations in the ESPI system is rigid body motion, which leads to fringes that are unrelated to the body deformations. In this study, the inward and outward

movement of the prism was tracked using an LVDT at the free end. One third of the results were excluded because of the presence of the rigid body motion, most with setup 1 where there is a weakness in the support because of the pre-stress release system. Modifications are recommended when using setup 1 in future studies to eliminate this prism movement.

A second limitation of the system is that the ESPI is a relative measuring technique. This means all of the displacements are calculated relative to a reference point which remains showing zero displacement. In this experiment, the reference point was chosen to be the middle of the concrete side-face. The ESPI measurements were then calibrated assuming the longitudinal displacement at the fixed end was zero.

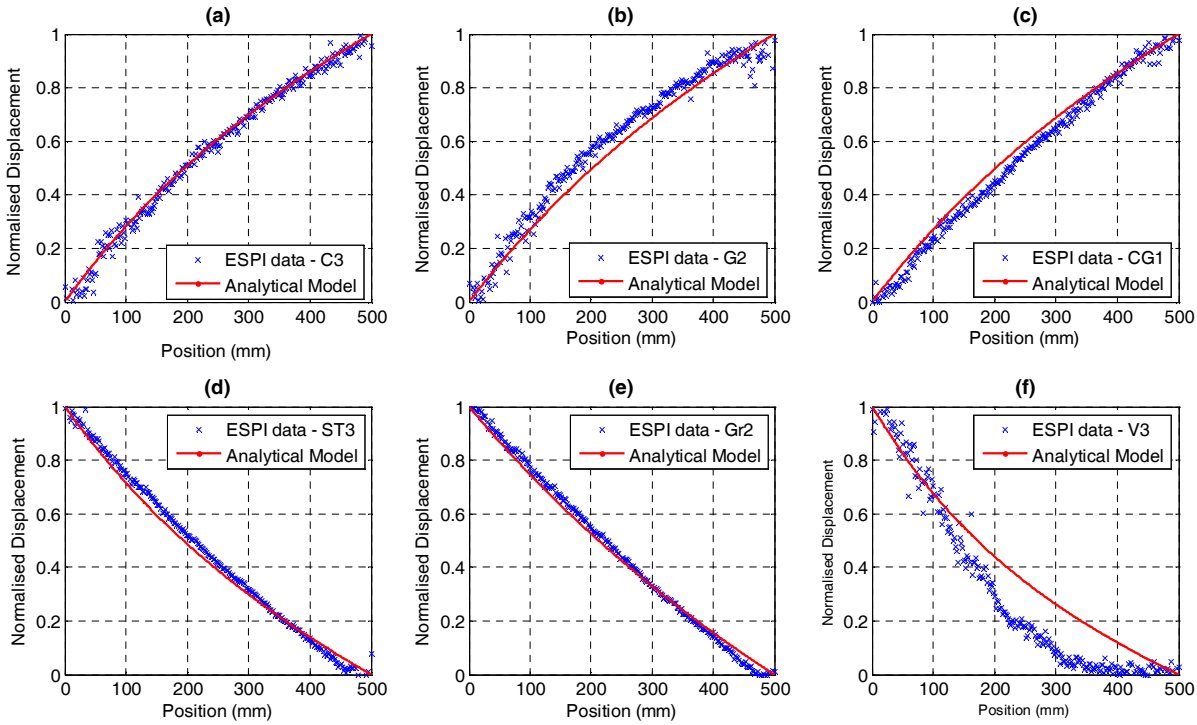

Figure 6: Normalised longitudinal displacement: (a) C3, (b) G2, (c) CG1, (d) ST3, (e) Gr2, (f) V3

Conclusions

An experimental validation of the re-anchorage model of the ruptured tendon in bonded post-tensioned concrete structures, which is proposed by authors in [2], was discussed in this paper. The experiments were conducted on thirty three post-tensioned concrete prisms utilising the 3D Electronic Speckle Pattern Interferometry (ESPI) to measure surface deformation.

The impact of the tendon's rupture was assessed by measuring longitudinal deformation of 0.5 metre concrete prisms after the rupture. The study shows that the ESPI system can provide rich and accurate information if rigid body motion is prevented through a well designed test setup.

The comparisons of results from the proposed model against these experimental results display good agreement. The proposed model is capable of simulating the re-anchoring phenomenon, and therefore, it can be used as an assessment tool to evaluate the structural capacity of post-tensioned concrete structures with ruptured tendons.

References

[1] Concrete Society, Durable bonded post-tensioned concrete bridges, in: Technical Report Technical Report 47 (TR47), 2002.
[2] A. O. Abdelatif, J. S. Owen, M. F. M. Hussein, Modeling the Re-anchoring of a Ruptured Tendon in Bonded Post-tensioned Concrete, in: Bond in Concrete 2012: Bond, Anchorage, Detailing, vol 1, Brescia, Italy, 2012, pp. 233-240.
[3] R. J. Woodward, F. W. Williams, Proceedings of the Institution of Civil Engineers Part 1-Design and Construction 84 (1988) 635-669.
[4] Highway Agency, The assessment of Concrete Structures affected by Steel Corrosion, in: T. H. Agency (Ed.) BA51/95: Design Manual for Roads and Bridges DMRB, vol.3, Section 4, Part 13 1995.
[5] S. H. Buchner, P. Lindsell, Testing of Prestressed Concrete Structures During Demolition, in: Structural assessment : the use of full and large scale testing, Butterworths, London ; Boston, 1987, pp. 46-54.
[6] D. G. Cavell, P. Waldron, Computers & Structures 79 (2001) 361-373.
[7] D. Coronelli, A. Castel, N. A. Vu, R. François, Engineering Structures 31 (2009) 1687-1697.
[8] C. A. Jeyasehar, K. Sumangala, Computers & Structures 84 (2006) 1709-1718.
[9] Y. H. Zeng, Q. H. Huang, X. L. Gu, W. P. Zhang, Experimental Study on Bending Behavior of Corroded Post-Tensioned Concrete Beams, in: vol 366, ASCE, Honolulu, HI, 2010, pp. 336-336.
[10] J. R. Janney, American Concrete Institute Journal 26 (1954) 736-731.
[11] R. I. Gilbert, N. C. Mickleborough, Design of prestressed concrete, E & FN Spon, London, 1990, p. xxii, 504 p.
[12] J. D. Geddes, I. Soroka, Effect of grout properties on transmission length in grout-bonded post-tensioned concrete beams, in: Magazine of Concrete Research, vol 16, Thomas Telford London, 1964, pp. 93-98.
[13] M. Schupack, D. W. Johnston, Journal of The American Concrete Institute 71 (1974) 522-525.
[14] S. Buchner, P. Lindsell, Testing of prestressed concrete structures during demolition, in: 1987.
[15] S. H. Buchner, P. Lindsell, Controlled Demolition of Prestressed Concrete Structures, in: Y. Kasai (Ed.) Demolition and reuse of concrete and masonry: Second International RILEM Symposium, vol 1, 1988, pp. 358-366.
[16] K. Watanabe, T. Tadokoro, Y. Tanimura, Quarterly Report of RTRI 52 (2011) 224-229.
[17] Tanaka Y., Kawano H., Watanabe H., K. T., Chloride-induced deterioration and its influence on load carrying capacity of post-tensioned concrete bridges, in: Third int. conf. concrete under severe conditions — Environment and loading, 2001, pp. p. 495–502.
[18] P. Hariharan, Basics of interferometry Elsevier Academic Press, Amsterdam ; Boston, 2007, p. xxi, 226 p.

Appendix A

Test No.	Prism ID	Stress (MPa)	Bar Dia. (mm)	Duct Material	Duct OD/T (mm)*	Concrete			Grout			Steel		Test setup	Remarks
						E	ft	fc	E	ft	fc	Es	fy		
1	P1	1020	7	PVC	20/1.9	31	3.6	57.1	26.8	2.1	68.9	207	1562	1	Plain concrete
	P2	1030													
	P3	1021													
2	P4	607.5	7	PVC	20/1.9	37.9	3.9	56.9	24.9	11.1	60.8	207	1562	1	
	P5	755.7													
	P6	815.7													
3	C1	783	7	PVC	20/1.9	43.2	3.8	50.6	23.7	7.5	47	207	1562	1	
	C2	880													
	C3	807.3													
4	G1	917.3	7	PVC	20/1.9	43.2	3.9	50.6	18.7	2.5	39	207	1562	1	
	G2	1032													
	G3	-													
5	CG1	866.5	7	PVC	20/1.9	43.4	3.6	46.1	19.2	9.5	31.7	207	1562	1	
	CG2	980.7													
	CG3	922.3													
6	CC1	872	7	PVC	20/1.9	43.9	3.62	46.6	-	-	51.7	207	1562	1	
	CC2	1090													
	CC3	832.4													
7	Dm1	900.4	7	Steel	19.05/1.59	44	4	49	8.53	12.7	53.7	207	1562	1	
	Dm2	837.3												2	
	Dm3	809.6													
8	C10	922	7	PVC	20/1.9	42.3	4.1	51.2	21	14.8	58.1	207	1562	2	
	C20	1098													
	C30	953													
9	ST1	861.5	7	PVC	20/1.9	44	4.5	52.5	25.1	12.4	71.6	207	1562	2	Reinforced concrete**
	ST2	979.7													
	ST3	953.4													
10	V1	1113	5	PVC	20/1.9	44.3	3.6	53.7	24.5	3.2	53.7	207	1562	2	Plain concrete
	V2	1062													
	V3	1096													
11	Gr1	801	7	PVC	20/1.9	44.6	2.7	46.8	13.2	3.8	15.2	207	1562	2	
	Gr2	983													
	Gr3	866													

*OD/T: Outer diameter/wall thickness

** Four 6 mm steel bars were used as main reinforcement with 6 mm stirrups every 50 mm

*** fc, ft, fy: compression, tensile, yield strength in MPa. E: Young's modulus in GPa